Tube-wave Effects in Cross-Well Seismic Data at Stratton Field

Valeri Korneev, Lawrence Berkeley National Laboratory, Jorge Parra, South-West Research Institute, Andrey Bakulin, Shell Int..

Summary

The analysis of crosswell seismic data for a gas reservoir in Texas revealed two newly detected seismic wave effects, recorded 2000 feet above the reservoir. The first is that the dominant late phases on the records are the tube waves generated in the source well and later converted into laterally propagating waves through the reservoir in gas/water saturated layers, which convert back to tube-waves in the receiver well. The tube-wave train showed good correlation with multilayered reservoir zone structure, suggesting that the recorded wave field has strong dependence on the reservoir parameters. The second effect is that the recorded field is composed of multiple low-velocity tube-waves. The modeling results suggest that imperfect cementation is the likely cause of this phenomenon.

Tube waves

Tube waves are traditionally regarded as a source of high amplitude noise in borehole seismic data and much effort typically goes into their suppression and elimination from recordings. Tube waves have very large amplitudes and can propagate long distances without substantial decay. A tube wave is an interface wave for a cylindrical interface between two media, typically a borehole fluid and surrounding elastic rock. Borehole waves were described by Lamb (1898) and were observed in the early twentieth century, as summarized by White (1965). Using trapped (or guided) mode analysis, the classic tube wave can be seen as the lowest order trapped mode (Schoenberg, 1981).

Stratton Field Experiment

The Stratton field experiment was designed in order to experimentally demonstrate the transmission and detection of guided waves in low-velocity sedimentary layers. The details of data acquisition, processing and low-velocity bed continuity study results can be found in Parra et. al. (2001). The objective of this project was to establish the feasibility and benefit of using interwell guided seismic waves in characterization of Gulf Coast gas reservoirs. Target zones were selected based on geological markers, seismic reflectors and well logs from the upper Frio Formation at the Stratton gas field. It was selected because it is one of the most extensively studied and well-documented producing oil and gas fields on the Gulf Coast. The Stratton field consists mainly of sandstones and shales of the Frio Formation with velocity contrasts on the order of 10% to 20%. Three low-velocity intervals were identified, from top to bottom, as the V2, V5, and V12 shale zones, and were recognizable in all the wells. The three wells used to conduct the interwell logging experiments and are located in almost the same vertical plane. The data were collected in the receiver wells Ward159 and Ward145, while sources were placed in the well Ward145 between the receiver wells at three positions, corresponding to the centers of target layers V2 at 3816 ft (A), V5 at 4133 ft (B) and V12 at 4570 ft (C). The source was Texaco's multiple air-gun array, a tool comprised of three air guns spaced 27 inches apart, which fire simultaneously with each shot.

The guided-wave signatures were related to targets arriving in the 0.6 – 0.8 s time interval. The strongest phases in the records, which were arriving later then 0.8 s were not interpreted at the time as being out of scope of the experiment goals.

Data sets

The Stratton three data sets A145, B145 and C145 consist of 46 records each from the receivers positioned across the target layers.

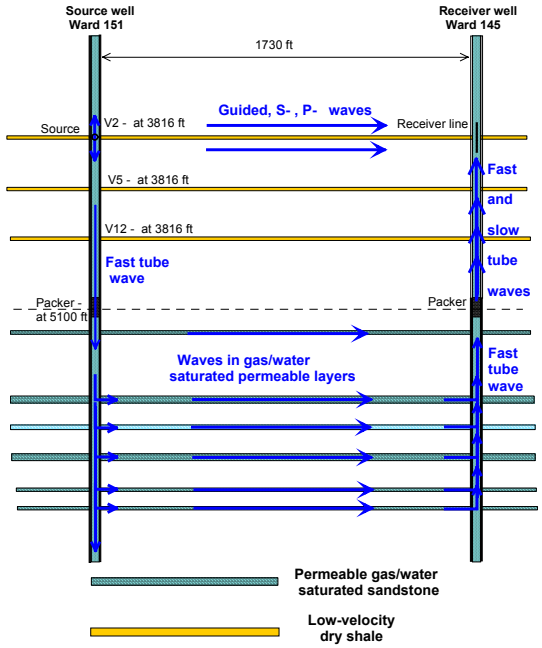

Figure 1. Cross-well experiment scheme and wave paths of the late arrivals.

The upper 7 receivers had a 10 ft spacing interval, while the next 33 receivers had 2 ft spacing and the lower 6 receivers again had 10 ft spacing interval. The recorded signal frequency was up to 300Hz in the well Ward145 and up to 100Hz in the far well Ward159. While geophones were used in the cemented well Ward159, the attempt to cement the space around the casing in the well Ward145 failed and there was no good bonding between the casing and the formations above 5100 ft in that well. On Figure 1 the low frequency (50-100Hz) filtered traces are shown for data sets A145, B145 and C145. There is a presence of late high amplitude arrivals in the data, which is most pronounced at low frequencies. These arrivals are concentrated in separate wavetrains, which are denoted as W_k , where the integer index $k = 1, 2, \ldots 6$ corresponds to the order of arrival.

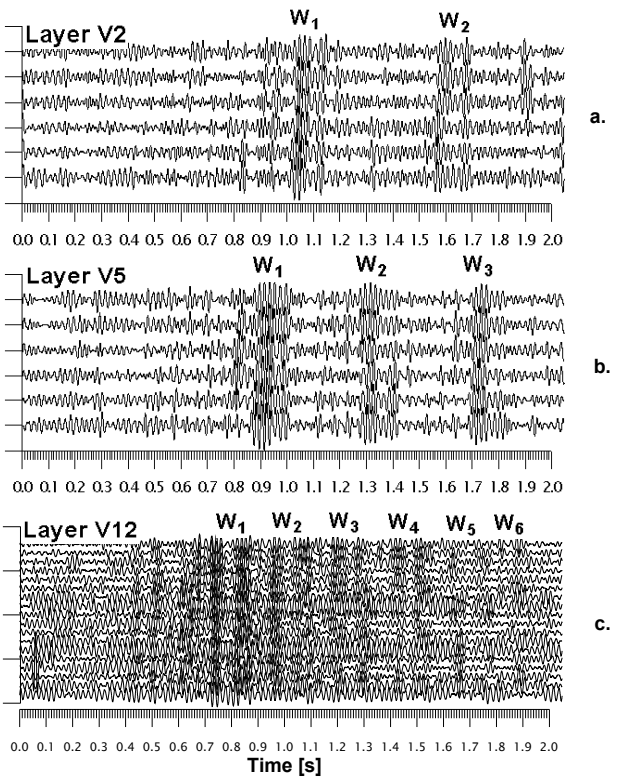

Figure 2. Cross-well low-band pass filtered data for 3 levels V2, V5, and V12. Visible are wavetrains Wn , n=1,6 for tube waves.

Data processing

The interpretation of the strong late phases arriving in the 0.8–2.0 s interval is the subject of this paper. The relatively small travel time (0.2s) for the direct P-wave arrivals suggests that the late phases belong to waves with long propagation paths and/or rather small velocities. This energy was clearly elsewhere while the direct P- waves were arriving at 0.2 s. The apparent velocities of the strongest phases around the 1 s arrival time were estimated to be in the 1300-1500 m/s range, which corresponds to propagating tube waves. The traces were cross–correlated with the corresponding first arriving wavetrain interval, which allowed the measurement of the main peak traveltimes with better than 0.01 s accuracy. This interval was 0.7 – 1.3 s for A145, 0.7 – 1.3 s for A145, and 0.7 – 1.3 s for A145 datasets. The high (90-100-200-220 Hz) and low (30-40-80-90 Hz) band-pass filtered data reveal practically the same results, which suggests negligibly low dispersion in the frequency band under consideration. The measured travel times for the strongest central peaks are given in Table 1 and represent upward propagating waves of varying velocities. The results for all tube-wave velocity evaluations are shown in Table 2. The almost perfect lateral homogeneity of the formation permits the interpretation of the wave propagation of late arrivals as consisting of three-leg paths. The wave propagates downward as a regular tube wave, then converts into a horizontally propagating wave along some seismically conductive layer and after reaching the receiver well it propagates upwards, splitting into a set of at least six waves of different velocities at packer depth. The depth h_g and velocity $\mathrm{v_g}$ of this horizontal layer may be estimated by solving two equations of the form

$$t_i^{(w)} = (2h_g - h_o - h_i)/\mathrm{v_c} + d_w/\mathrm{v_g} + (h_o - h_i)/\mathrm{v_1}, \quad (1)$$

where $t_i^{(w)}$ is the travel time of a first arriving tube wave at both receiver wells ($w = 159,\ 145$), and $\mathrm{d_w}$ is the distance between source and receiver wells ($\mathrm{d_{159}} = 2740$ ft., $\mathrm{d_{145}} = 1730$ ft.). Three independent estimates for each target layer $i = A, B, C$ gave the values $h_g = 5717$ ft. After obtaining these estimates, equation (1) can be used to map the recorded seismic phases from the time to the depth scale.

Tube wave modeling

A solution for axial wave propagation in a layered cylinder was used to explain the observed phenomena of tube-wave splitting. The solution is exact and expressed in form of an independent mode series with integer index m. For any given frequency ω and mode index m the tube-wave velocities $v_{tw}^{(m)}$ were found as the real roots of

Receiving wells ->	Ward 159	Ward 151					
Recorded waves	Wave 1	Wave 1	Wave 2	Wave 3	Wave 4	Wave 5	Wave 6
Layer V2 at 3816 ft	1.17	1.055	1.605	-	-	-	-
Layer V5 at 4133 ft	1.04	0.92	1.32	1.75	-	-	-
Layer V12 at 4570 ft	0.86	0.73	0.965	1.19	1.115	1.64	1.875

Table 1. Picked travel times [s] for the maximum energy phases.

Cemented wells	Non cemented part above casing in Ward 151					
Wave 1	Wave 1	Wave 2	Wave 3	Wave 4	Wave 5	Wave 6
1460	1365	470	288	207	162	132

Table 2. Tube-wave velocities [m/s].

$\Delta_m(v_{tw}^{(m)}, \omega) = 0$, where $\Delta_m(v_{tw}^{(m)}, \omega)$ is the determinant of a corresponding boundary condition problem. The primary purpose of the modeling is the explanation of the six different tube-wave propagation velocities found in the Stratton experiment data. The diameter of the drill bit for this well was 25 cm and the diameter of the steel casing was 10 cm. These values, as well as the known material parameters for water, steel casing and the outer rock formation were kept unchanged.

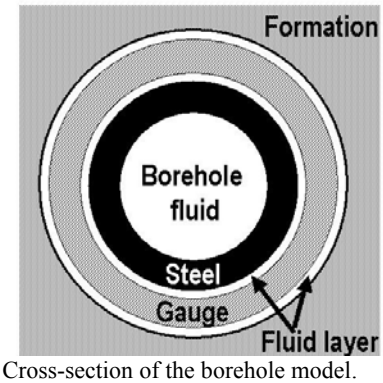

Figure 3 Cross-section of the borehole model.

The quality of bonding between the casing and the outer rock in receiver well Ward145 is under investigation because this well is not cemented above the packer at 5100 ft. This material will be henceforth referred to as *gauge*, implying that it represents a poorly consolidated, liquid saturated mixture of sand and shale that contains gas, as the formation has some gas bearing layers.

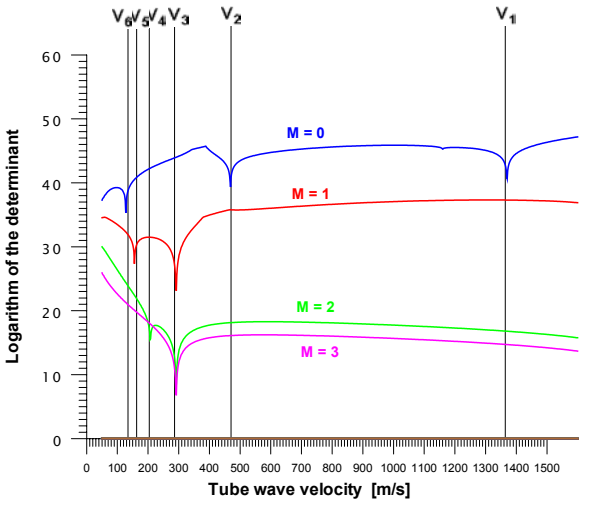

Figure 4 Determinants of dispersion equation for cylindrical layered model. Vertical lines mark measured velocities of tube waves.

Several models were used in an attempt to match the observed tube-wave data, including different types of space fillings around the casing: all possible combinations of low velocity gauge, which had either welded or sliding contacts with adjacent layers, and could also have thin liquid intermediate *skin* layers that separate gauge from casing or rock. The results of computations suggest that the velocities of wave trains W_2 and W_3 are practically equal to the compressional and shear velocities of the gauge correspondingly.

This conclusion is supported by a typical value of v_s / v_p ratio equal to 0.62 for these two waves, and also by a perfect fit for the fastest velocity of W_1. The thicknesses of the liquid layers had strongest impact on the velocities of W_4, W_5 and W_6, and were varied to find the best fit. The best fit for one out of the nine possible models is presented in Figure 2. The only model which provides a good fit for all velocities observed in the experiment has sliding contact between casing and the gauge and 7 mm thick liquid skin layer separating the gauge from the host rock formation. All gauge-containing models show the fastest tube-wave velocity to be about 6% lower than in the cemented case. Sliding–welded and welded-sliding contact models revealed just the main root for the fastest velocity. The sliding-sliding pair gave just two roots for W_5 and W_6, but these two roots were absent for the liquid skin containing models.

Discussion

The recorded travel times of the tube waves consistently indicate that the well packer was the source of slow tube-wave generation. The cement packer represents a strong diffractor that converts the fundamental (fastest) tube wave into a set of slower waves, exciting an additional fundamental mode (m=0) related to the gauge and two modes (m=1) related to the liquid layer. Such waves for parallel-layer models were detected and explained by Chouet (1986) and Ferrazini and Aki (1987). They showed that waves propagating in a liquid layer between two adjacent halfspaces can have arbitrarily low velocities, which depend on the thickness of the layer. In the case of the cylindrical model, the velocity of waves in the liquid layers showed detectable sensitivity to changes as low as 1 mm in the liquid layer thickness. It seems unlikely, thought, that liquid skin layer model is an accurate representation of reality. It seems more likely that small pockets of water trapped in the gauge effectively act as a single thin layer. This is partially supported by the presence of low velocity tube-waves for the models containing a liquid layer on either side of the gauge.

Conclusions

Because reservoir waves should be affected by reservoir properties (i.e. porosity, permeability, fracture density and orientation), monitoring based on use of these waves should allow the detection and interpretation of reservoir property changes near production boreholes. These effects can be used for the development of new and promising technology for the imaging and monitoring of underground gas, oil and water reservoirs.

References

Chouet B., 1986. Dynamics of a fluid-driven crack in three dimensions by the finite difference method. J. Geophys. Res., **91**, 13967-13992

Ferrazini and Aki, 1987. Slow waves trapped in fluid-filled infinite-crack: implication for volcanic tremor. J. Geophys. Res., **92**, B9, 9215-9223.

Lamb, H., 1898, On the velocity of sound in a tube, as affected by the elasticity of the walls: Manchester Memoirs, **42**, 1-16.

Parrra, J.O., Hackert, C., Gorogy, A and Korneev, V. A, 2001, Detection of guided waves between gas wells for reservoir characterization, Geophysics, Vol.67, No 1, p. 38-49, LBNL-48523.

Schoenberg, M., Marzetta, T., Aron, J., Porter, R.P., Space-time dependence of acoustic waves in a borehole: J. Acoust. Soc. Am., **70**, 1496-1507.

White, J.E., 1965, Underground soung, McGraw-Hill, Inc., 302p.

Acknowledgments

This work was spported by the Office of Science, Office of Basic Energy Sciences, Division of Engineering and Geosciences of the U.S. Department of Energy under Contract No.DE-AC03-76SF00098. It was also supported by Shell Int. The data were obtained with support of the Gas Research Institute, contract 5093-260-2600. Authors wish to thank Anthony Gorody for fruitful discussions and collaboration in experiment planning and data acquisition.